Carcinogenesis vol.33 no.4 pp.876–885, 2012
doi:10.1093/carcin/bgs097
Advance Access publication February 3, 2012

Intervention of human breast cell carcinogenesis chronically induced by 2-amino-1-methyl-6-phenylimidazo[4,5-b]pyridine

Shambhunath Choudhary[1,2], Shilpa Sood[1,2], Robert L.Donnell[2] and Hwa-Chain R.Wang[1,2,*]

[1]Anticancer Molecular Oncology Laboratory and [2]Department of Biomedical and Diagnostic Sciences, College of Veterinary Medicine, The University of Tennessee, Knoxville, TN 37996, USA

[*]To whom correspondence should be addressed. Tel: +1 865 974 3846; Fax: +1 865 974 5640;
Email: hcrwang@utk.edu

More than 85% of breast cancers are sporadic and attributable to long-term exposure to environmental carcinogens, such as those in the diet, through a multistep disease process progressing from non-cancerous to premalignant and malignant stages. The chemical carcinogen 2-amino-1-methyl-6-phenylimidazo[4,5-b]pyridine (PhIP) is one of the most abundant heterocyclic amines found in high-temperature cooked meats and is recognized as a mammary carcinogen. However, the PhIP's mechanism of action in breast cell carcinogenesis is not clear. Here, we demonstrated, for the first time, that cumulative exposures to PhIP at physiologically achievable, pico to nanomolar concentrations effectively induced progressive carcinogenesis of human breast epithelial MCF10A cells from a non-cancerous stage to premalignant and malignant stages in a dose- and exposure-dependent manner. Progressive carcinogenesis was measured by increasingly- acquired cancer-associated properties of reduced dependence on growth factors, anchorage-independent growth, acinar-conformational disruption, proliferation, migration, invasion, tumorigenicity with metastasis and increased stem-like cell populations. These biological changes were accompanied by biochemical and molecular changes, including upregulated H-Ras gene expression, extracellular signal-regulated kinase (ERK) pathway activation, Nox-1 expression, reactive oxygen species (ROS) elevation, increased HIF-1α, Sp1, tumor necrosis factor-α, matrix metalloproteinase (MMP)-2, MMP-9, aldehyde dehydrogenase activity and reduced E-cadherin. The Ras-ERK-Nox-ROS pathway played an important role in not only initiation but also maintenance of cellular carcinogenesis induced by PhIP. Using biological, biochemical and molecular changes as targeted endpoints, we identified that the green tea catechin components epicatechin-3-gallate and epigallocatechin-3-gallate, at non-cytotoxic doses, were capable of suppressing PhIP-induced cellular carcinogenesis and tumorigenicity.

Introduction

Human breast cancer is the most common type of cancer and the second leading cause of cancer deaths among women in northern America and Europe (1). More than 85% of breast cancers are sporadic and attributable to long-term exposure to environmental factors through a multi-year and multistep disease process progressing from non-cancerous to premalignant and malignant stages (2,3). More than 200 chemical mammary carcinogens have been detected by the existing experimental paradigm that uses high doses of carcinogens (micro to millimolar concentrations) to induce cancerous cells in cultures and tumors in animals as steps in evaluating the potency of carcinogens (3–5). However, since long-term exposure to low doses of carcinogens is responsible for most human cancers, a high-dose approach may not be a proper way to reveal the effect of environmental carcinogens in breast cancer development. Thus, an urgent need exists to take a new approach of validating carcinogens, at physiologically achievable levels, effective in chronic induction of human breast cell carcinogenesis and then identifying preventive agents capable of intervening.

The dietary carcinogen 2-amino-1-methyl-6-phenylimidazo[4,5-b]pyridine (PhIP) is one of the most mass abundant heterocyclic amines, which are particularly found in high-temperature cooked meats, such as grilled/barbequed meats (6–8). Epidemiological studies indicate that an increased risk of breast cancer is closely associated with increased consumption of PhIP in well-done meats (9,10). Human consumption of PhIP at microgram levels results in systemic PhIP exposure at pico to low nanomolar levels (8). Studies in rats revealed that daily gastric administration of PhIP in milligram ranges induces mammary tumors (8). Studies of genotoxicity to human cell lines and adduct formation reveal genotoxic activity of PhIP at a concentration as low as 450 nmol/l (8,11). However, whether long-term exposure of breast cells to PhIP at physiologically achievable pico to low nanomolar levels may induce carcinogenesis and tumorigenicity remains to be clarified.

Daily, oral administration of PhIP at 75 mg/kg into rats for 10 days induces intraductal proliferation, carcinoma *in situ* and carcinoma with increased frequencies of activation mutations within the H-*ras* gene (12). Expression of oncogenic H-Ras in immortalized, non-cancerous human breast epithelial MCF10A cells induces an invasive phenotype, accompanied by expression of matrix metalloproteinase-2 and -9 (MMP-2 and -9) (13) and extracellular signal-regulated kinase (ERK) pathway activation (14). Activation of the ERK pathway leads to reduced nicotinamide adenine dinucleotide phosphate oxidase-1 (Nox-1) expression, and Nox-1 mediates reactive oxygen species (ROS) elevation, which plays an important role in cell proliferation, motility, invasion and angiogenesis (14,15). It has been shown that a single exposure of MCF10A cells to PhIP at nanomolar concentrations induces cell proliferation and transient activation of the ERK pathway (16). However, the role of transient ERK pathway activation in PhIP-induced carcinogenesis remains to be clarified. It is well recognized that transition activation of the ERK pathway, which consists of Raf, Mek and Erk, contributes to cell proliferation, survival and differentiation, and constant activation of the ERK pathway leads to malignant transformation (17). Whether long-term exposure to PhIP results in constant activation of the Ras-ERK-Nox-ROS pathway for cellular carcinogenesis remains to be determined.

We developed a cellular model to mimic chronic induction of human breast cell carcinogenesis associated with accumulated exposures to low doses of environmental carcinogens, such as 4-(methylnitrosamino)-1-(3-pyridyl)-1-butanone (NNK) and benzo[a]pyrene (18–21). We have used various transient and constitutive endpoints as targets to identify preventive agents, such as green tea catechins, effective in suppression of cellular carcinogenesis (19–22). Green tea catechins include four major components: epicatechin, epicatechin-3-gallate (ECG), epigallocatechin and epigallocatechin-3-gallate (EGCG) (23). These components, at a non-cytotoxic concentration of 10 μg/ml, suppress cellular carcinogenesis chronically induced by NNK and benzo[a]pyrene (22). However, whether these catechins are effective in suppression of PhIP-induced cellular carcinogenesis remains to be studied.

In this communication, we used our model to clarify the carcinogenic activity of PhIP, at physiologically achievable doses, in inducing progressive carcinogenesis of MCF10A cells from a non-cancerous stage to premalignant and malignant stages. We revealed that the Ras-ERK-Nox-ROS pathway played an important role in both

Abbreviations: ALDH, aldehyde dehydrogenase; CM, complete medium; DPI, diphenylene iodonium; ECG, epicatechin-3-gallate; EGCG, epigallocatechin-3-gallate; ERK, extracellular signal-regulated kinase; MMP, matrix metalloproteinase; NAC, N-acetyl-L-cysteine; PhIP, 2-amino-1-methyl-6-phenylimidazo[4,5-b]pyridine; ROS, reactive oxygen species; siRNA, small interfering RNA; TNF, tumor necrosis factor; wt, wild-type.

initiation and maintenance of cellular carcinogenesis chronically induced by PhIP. We used various transient and constitutive endpoints as targets to identify that ECG and EGCG, at non-cytotoxic levels, were effective in suppression of PhIP-induced cellular carcinogenesis and tumorigenicity.

Materials and methods

Cell cultures and reagents

MCF10A (American Type Culture Collection, Rockville, MD) and derived cell lines were maintained in complete (CM) medium (1:1 mixture of Dulbecco's modified Eagle's medium and Ham's F12, supplemented with 100 ng/ml cholera enterotoxin, 10 μg/ml insulin, 0.5 μg/ml hydrocortisol, 20 ng/ml epidermal growth factor and 5% horse serum) (18–21). Human breast cancer MCF7 and urinary bladder cancer J82 cells (American Type Culture Collection) were maintained in Dulbecco's modified Eagle's medium supplemented with 10% heat-inactivated fetal calf serum (21,24). All cultures were maintained in medium supplemented with 100 U/ml penicillin and 100 μg/ml streptomycin in 5% CO_2 at 37°C. Stock aqueous solutions of PhIP (Midwest; NCI Chemical Carcinogen Reference Standard Repository), chloromethyl dichlorodihydrofluorescein diacetate (Invitrogen, Carlsbad, CA), U0126 (Cell Signaling, Beverly, MA) and diphenylene iodonium (DPI) (Acro, Morris Plains, NJ) were prepared in dimethyl sulfoxide and diluted in culture medium. Stock aqueous solutions of epicatechin, ECG, epigallocatechin, EGCG (Sigma–Aldrich, St Louis, MO) and *N*-acetyl-L-cysteine (NAC) (Alexis, San Diego, CA) were prepared in H_2O and diluted in culture medium for assays.

Chronic induction of cellular carcinogenesis

To chronically induce cellular carcinogenesis, 24 h after each subculturing, MCF10A cultures were treated with PhIP for 48 h as one cycle of exposure for 5–20 cycles; cultures were subcultured every 3 days (21).

Reduced dependence on growth factors

A total of 3×10^3 cells were seeded in 60 mm culture dishes and maintained in low-mitogen medium, containing reduced total serum and mitogenic additives to 2% of the concentration formulated in CM medium, for 10 days to develop cell colonies (21).

Anchorage-independent growth

A total of 3×10^3 cells were mixed with soft agar consisting of 0.4% SeaPlaque agarose (Sigma–Aldrich) in a mixture (1:1) of CM medium with 3 day conditioned medium prepared from MCF10A cultures, plated on top of the 2% SeaPlaque agarose base layer in 60 mm culture dishes and maintained for 14 days to develop cell clones (21).

Acinar-conformational disruption

A total of 3×10^3 cells were mixed with CM medium containing 4% Growth Factor-Reduced Matrigel Matrix (BD Biosciences), plated on Matrigel base in each well of 24-well culture plates and maintained for 14 days to develop spheroids (21).

Cell proliferation

Cell proliferation was determined using the 5-bromo-2′-deoxyuridine cell proliferation enzyme-linked immunosorbent assay kit (Roche, Indianapolis, IN); quantification of 5-bromo-2′-deoxyuridine-labeled cells was determined with an enzyme-linked immunosorbent assay reader (Bio-Tek), as performed previously (24).

In vitro *cell invasion and migration*

The cell invasion assay was performed using 24-well transwell insert chambers with a polycarbonate filter with a pore size of 8.0 μm (Costar, Corning, NY). A total of 2×10^4 cells in serum-free medium were seeded on top of a Matrigel-coated filter (BD Biosciences) in each insert chamber. Then, insert chambers were placed into wells on top of culture medium containing 10% horse serum as a chemoattractant. The migration assay was performed using 24-well transwell insert chambers with a polycarbonate filter without Matrigel. The invasive or migratory ability of cells was determined by the number of cells translocated to the lower side of filters (25).

Serum-independent non-adherent growth

A total of 1×10^4 cells were seeded on top of 1% agarose-coated, non-adherent 100 mm culture plates, incubated in serum-free MCF10A medium supplemented with 0.4% bovine serum albumin and maintained for 10 days to develop mammospheres (26).

Aldehyde dehydrogenase

An ALDEFLUOR Kit (StemCell Technologies, Durham, NC) was used to detect aldehyde dehydrogenase (ALDH)-positive cells. Cells were mixed with activated Aldefluor substrate BODIPY-aminoacetaldehyde and incubated in the presence and absence of the ALDH inhibitor diethylaminobenzaldehyde, followed by flow cytometric analysis (24). The mean fluorescence intensity of cells was quantified using Multicycle software (Phoenix Flow System, San Diego, CA). Cells incubated with BODIPY-aminoacetaldehyde in the presence of diethylaminobenzaldehyde were used to establish the baseline of fluorescence for determining the ALDH-positive cell population in which ALDH activity was not inhibited by diethylaminobenzaldehyde (26).

Intracellular ROS

Cells were incubated with 5 μmol/l chloromethyl dichlorodihydrofluorescein diacetate in 5% CO_2 at 37°C for 1 h to detect ROS level by flow cytometric analysis; the mean fluorescence intensity of dichlorodihydrofluorescein was quantified using Multicycle software (Phoenix Flow System), as performed previously (14).

DNA damage

DNA damage was measured by a comet assay. Cells were trypsinized and collected in phosphate-buffered saline at a density of 2×10^4 cells/ml. Cell suspension was mixed with an equal volume of 1% low-melting agarose (Fisher, Fair Lawn, NJ) and placed on agarose-coated slides. Slides were then immersed in lysis solution (1.2 mol/l NaCl, 100 mmol/l Na_2-ethylenediaminetetraacetic acid, 1% Triton X-100 and 0.3 nmol/l NaOH, pH 13) at 25°C for 1 h and rinsed three times with alkaline buffer (2 mmol/l Na_2-ethylenediaminetetraacetic acid and 300 mmol/l NaOH) for 20 min each. After electrophoresis in the same alkaline buffer at 20 V for 30 min (27), slides were stained with 2.5 μg/ml of propidium iodide for 20 min and examined with a Zeiss fluorescence microscope (Carl Zeiss Inc, Thornwood, NY) equipped with an excitation filter of 546 nm and barrier filter of 590 nm. Fifty nuclei per slide were scored for tail moment (% of DNA in the tail × tail length) as a parameter using CometScore software (Tritek).

Downregulation by small interfering RNAs

Validated human H-Ras-specific (sc-29340) and Nox-1-specific (sc-43939) small interfering RNAs (siRNAs) (Santa Cruz Biotechnology, Santa Cruz, CA) are pools of three to five sequence-specific 19–25 nt siRNAs designed to knock down gene expression. Cells were transfected with 80 pmol/l H-Ras-specific, Nox-1-specific or control siRNAs (sc-37007) in antibiotic-free medium using siRNA transfection reagent (sc-29528).

Reverse transcription–PCR

Total RNA isolated from cultures using the Absolutely RNA kit (Stratagene, La Jolla, CA) was reverse transcribed to complementary DNA using a Verso cDNA Kit (Thermo Scientific, Waltham, MA). The resulting complementary DNAs were subjected to PCR for H-Ras (forward: 5′-GACGGAATATAAGCTGGTGG-3′; reverse: 5′-AGGCACGTCTCCCCATCAAT-3′) and β-actin (forward: 5′-GGACTTCGAGCAAGAGATGG-3′; reverse: 5′-AGCACTGTGTTGGCGTACAG-3′). PCR products were electrophoresed on agarose gels and visualized after ethidium bromide staining.

Western immunoblotting

Equal amount of cellular proteins were resolved by electrophoresis in either 10 or 14% sodium dodecyl sulfate–polyacrylamide gels and transferred to nitrocellulose filters for western immunoblotting, as described previously (21,24), using specific antibodies to detect H-Ras, Raf-1, phosphorylated Erk1/2 (p-Erk1/2), Erk1/2, Nox-1, p53, tumor necrosis factor (TNF)-α, MMP-2, MMP-9, E-cadherin, vascular endothelial growth factor, Sp1, β-actin (Santa Cruz Biotechnology), p-Raf-1, p-Mek1/2, Mek1/2, p-H2AX, H2AX and HIF-1α (Cell Signaling). Antigen–antibody complexes on filters were detected by the Supersignal chemiluminescence kit (Pierce, Rockford, IL).

Tumorigenicity and histopathology

Cells were mixed with Matrigel basement membrane matrix (BD Biosciences), and 1×10^7 cells in 100 μl were injected into the inguinal mammary fat pads of 10-week-old female athymic NCr-nu/nu mice (National Cancer Institute, Frederick, MD). Each group of four mice was maintained under pathogen-free conditions. Animals were monitored every 3 days. Xenograft tumor tissues were immediately harvested after euthanasia by exposure to CO_2. Tumor tissues were fixed in neutral-buffered formalin and embedded in paraffin for histopathological evaluation. Tumor tissue lysates were prepared to detect various proteins using western immunoblotting (24). All animal procedures were approved by The University of Tennessee Animal Care and Use Committee and were in accordance with the National Institutes of Health Guide for the Care and Use of Laboratory Animals (National Research Council, 1985).

Immunohistochemistry

Immunohistochemistry procedures were performed on paraffin-embedded tissue sections. Briefly, 5 μm tissue sections were adhered to charged glass slides, deparaffinized and pre-soaked in Tris-buffered saline/Tween for 10 min (24). Immunohistochemistry staining was carried out on an Autostainer (Dako, Carpinteria, CA), following a procedure of peroxide blocking for 5 min, serum-free protein blocking for 30 min, exposure to rabbit anti-human TNF-α antibody for 30 min and Dako Envision with horseradish peroxidase anti-rabbit treatment and chromagen labeling with Dako diaminobenzidene + for 30 min. The sections were then counterstained with hematoxylin for microscopic evaluation.

Statistical analysis

The Student's *t* test was used to analyze statistical significance, indicated by $^{*}P < 0.05$, $^{**}P < 0.01$ and $^{***}P < 0.001$; a *P* value of ≤0.05 was considered significant.

Results

Dose- and exposure-dependent induction of carcinogenesis by PhIP

To investigate the activity of PhIP in chronic induction of human breast cell carcinogenesis, we repeatedly exposed MCF10A cells to PhIP for 20 cycles. Then, we used two cancer-associated properties to measure the progress of cellular carcinogenesis. When cells acquire reduced dependence on growth factors and the ability of anchorage-independent growth during tumorigenic transformation, their survivability is aberrantly increased; for normal cells to grow and survive, growth factors are required, and cell adhesion to extracellular matrixes is important for cell survival in a multicell environment (28–30). As shown in Figure 1A and B, accumulated exposures to PhIP at 1 pmol/l for 20 cycles or 10 pmol/l for 5 cycles induced significant increases of cell clones acquiring both cancer-associated properties. These results verified that cumulative exposures to PhIP induced progression of cellular carcinogenesis in a dose- and exposure-dependent manner.

Investigating signaling pathways involved in PhIP-induced cellular carcinogenesis, we detected that H-Ras and Nox-1 protein level and phosphorylation of Raf-1, Mek1/2 and Erk1/2 were constantly increased in cells exposed to PhIP in a dose-dependent manner (Figure 1C). These results indicate that H-Ras and Nox-1 expression and activation of the ERK pathway were induced in concert with PhIP-induced cellular carcinogenesis.

Because 10 nmol/l PhIP, a physiologically achievable level in humans (8), was effective in inducing carcinogenesis progression and the Ras-ERK-Nox pathway, we used this concentration in the following studies.

Constitutive endpoints induced by PhIP in carcinogenesis

To further investigate PhIP-induced progressive carcinogenesis, we repeatedly exposed MCF10A cells to 10 nmol/l PhIP for 10 and 20 cycles, resulting in MCF10A-10nM-P10 (P-10) and -P20 (P-20) cells, respectively. Using tumorigenic MCF10A-Ras cells, an MCF10A-derived cell line in which oncogenic H-Ras is ectopically expressed (14,31), as a malignant control, we studied the cancer-associated properties of acinar-conformational disruption; cell proliferation, migration and invasion; reduced dependence on growth factors and anchorage-independent growth. Acinar structures with a hollow lumen and apicobasally polarized cells are important characteristics found in glandular epithelia *in vivo*; disruption of an intact glandular structure is a hallmark of epithelial carcinogenesis (32). As we demonstrated previously (19–21), non-cancerous MCF10A cells form mainly regular spheroids with acinar structures with a hollow lumen and apicobasally polarized cells on Matrigel, but breast cancer MCF7 cells form mainly irregular spheroids with filled luminal space lacking apicobasal polarity (19–21). Increased rates of cell proliferation and increased cell migration and invasion are closely associated with cell malignancy (28,33). As shown in Figure 2A, P-20 cells acquired significantly higher degrees of these cancer-associated properties than P-10 cells and either comparable or modestly lower degrees of these properties than MCF10A-Ras cells, indicating that cumulative exposures to PhIP resulted in progressively increased acquisition of distinctive cancer-associated properties; these quantifiable properties may be regarded as constitutive biological targeted endpoints for measuring the progress of carcinogenesis chronically induced by PhIP.

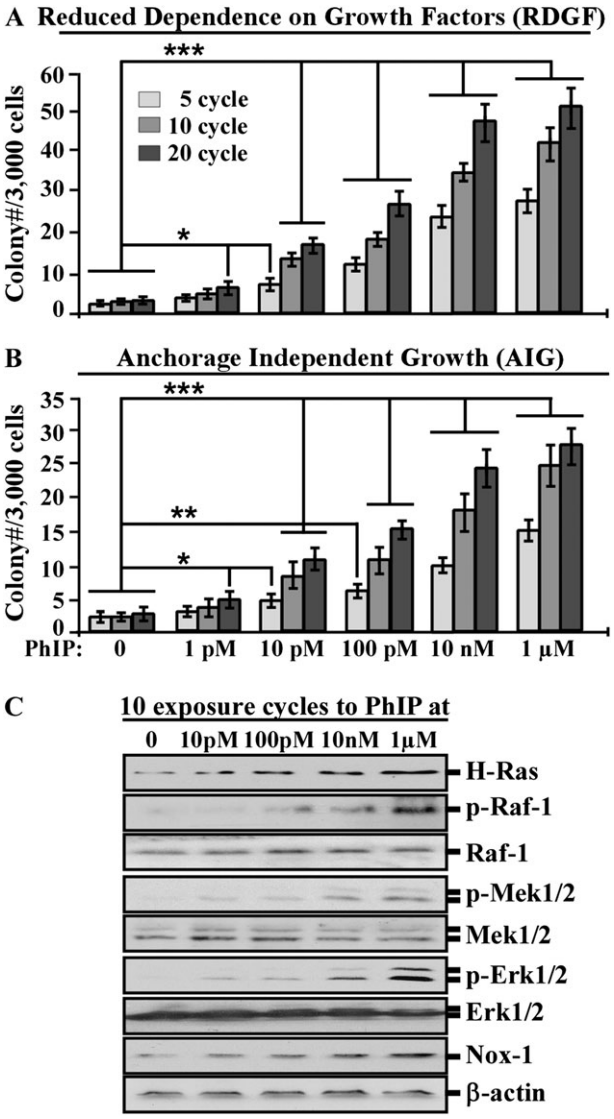

Fig. 1. Dose- and exposure-dependent induction of carcinogenesis by PhIP. MCF10A cells were repeatedly exposed to dimethyl sulfoxide (0) or 1, 10 and 100 pmol/l (pM); 10 nmol/l (nM) and 1 μmol/l (μM) PhIP for 5, 10 and 20 cycles. (**A**) To determine acquisition of the cancer-associated property of reduced dependence on growth factors (RDGF), cells were maintained in low-mitogen medium for 10 days. (**B**) To determine acquisition of the cancer-associated property of anchorage-independent growth (AIG), cells were seeded in soft agar for 14 days. Cell colonies (≥0.5 mm diameter) grown in low-mitogen medium and soft agar were counted microscopically. Columns, mean of triplicates; bars, standard deviation. The Student's *t* test was used to analyze statistical significance, indicated by $^{*}P < 0.05$, $^{**}P < 0.01$ and $^{***}P < 0.001$. (**C**) Lysates from cells exposed to PhIP for 10 cycles were prepared and analyzed by western immunoblotting using specific antibodies to detect levels of H-Ras, phosphorylated Raf-1 (p-Raf-1), Raf-1, p-Mek1/2, Mek1/2, p-Erk1/2, Erk1/2 and Nox-1, with β-actin as a control. All results are representative of three independent experiments.

Although investigating signaling pathways modulated in PhIP-induced progressive carcinogenesis, we detected that progressively increased levels of H-Ras protein, phosphorylated Erk1/2, Nox-1 protein and ROS (Figure 2B) coincided with increased degrees of

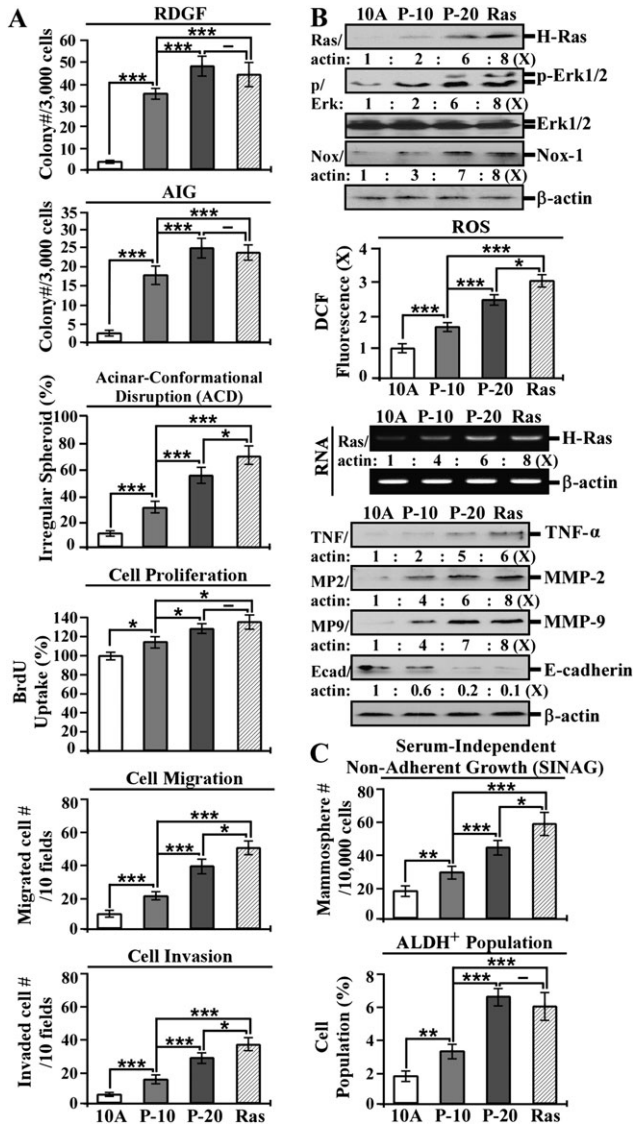

Fig. 2. Constitutive targeted endpoints in progressive carcinogenesis induced by PhIP. MCF10A (10A) cells were repeatedly exposed to 10 nmol/l PhIP for 10 and 20 cycles, resulting in the MCF10A-10nM-P10 (P-10) and -P20 (P-20) cell lines, respectively. MCF10A cells were stably transfected to ectopically express oncogenic H-Ras, resulting in the MCF10A-Ras cell line (Ras). (**A**) Cells were maintained in low-mitogen medium for 10 days, seeded in soft agar for 14 days and seeded in Matrigel for 14 days to determine cellular acquisition of reduced dependence on growth factors (RDGF), anchorage-independent growth (AIG) and acinar-conformational disruption (ACD), respectively. Cell colonies (≥0.5 mm diameter) grown in low-mitogen medium and soft agar were counted. Regular and irregular spheroids in Matrigel were counted, and the percentage of irregular spheroids was calculated. Cell proliferation was determined; relative cell growth rate was normalized by the value of 5-bromo-2′-deoxyuridine detected in 10A cells, set as 100%. Migratory and invasive activities were determined by counting the numbers of cells translocated through a polycarbonate filter without or with coated Matrigel, respectively in 10 arbitrary visual fields. (**B**) Cell lysates were analyzed by western immunoblotting using specific antibodies to detect levels of H-Ras, phosphorylated Erk1/2 (p-Erk1/2), Erk1/2, Nox-1, TNF-α, MMP-2, MMP-9 and E-cadherin, with β-actin as a control. The levels of H-Ras, Nox-1, TNF-α, MMP-2, MMP-9 and E-cadherin were calculated by normalizing with the level of β-actin, the level set in 10A cells as 1 (X, arbitrary unit). The level of specific phosphorylation of Erk1/2 (p/Erk) was calculated by normalizing the level of p-Erk1/2 with the level of Erk1/2, then the level set in 10A cells as 1 (X, arbitrary unit). ROS levels were measured with chloromethyl dichlorodihydrofluorescein diacetate labeling; relative level of ROS, as fold induction (X, arbitrary unit), was normalized by the level determined in 10A cells, set as 1. Total RNAs (RNA) were isolated and analyzed by PCR with specific primers to determine relative gene expression levels of H-Ras with β-actin as a control. (**C**) To determine serum-independent non-adherent growth (SINAG), cells were seeded in non-adherent cultures for 10 days and mammospheres (≥0.1 mm diameter) were counted. Mammospheres were collected and trypsinized, and ALDH-expressing (ALDH+) cell population (%) was measured by flow cytometry. Columns, mean of triplicates; bars, standard deviation. The Student's *t* test was used to analyze statistical significance, indicated by $^{*}P < 0.05$, $^{**}P < 0.01$ and $^{***}P < 0.001$. All results are representative of three independent experiments.

cancer-associated properties (Figure 2A). We also detected that H-*ras* gene expression was progressively upregulated in P-10 and P-20 cells (Figure 2B). However, sequencing of complementary DNA derived from the H-*ras* transcript did not detect any mutations, indicating mutational activation of the H-*ras* gene was not induced in PhIP-induced chronic carcinogenesis of breast cells. Thus, it appears that cumulative exposures to PhIP resulted in constantly elevated wild-type (wt) H-*ras* gene expression and protein, leading to activation of downstream ERK pathway and Nox-1 and ROS elevation. Induction of Nox-1 leads to ROS production, and ROS elevation is important in cell proliferation and malignant transformation (34,35). However, whether constant upregulation of wt H-Ras was sufficient to maintain PhIP-induced cellular carcinogenesis and ERK pathway activation to ROS elevation needs to be addressed.

Continuing our investigation of signaling modulators downstream from the ERK pathway, we detected progressive increases of TNF-α, MMP-2 and MMP-9 as well as progressive decreases of E-cadherin (Figure 2C) that were consistent with the increased degrees of acquired migratory and invasive activities by P-10, P-20 and MCF10A-Ras cells (Figure 2A). It has been reported that TNF-α promotes invasion and metastasis of breast carcinoma cells via increasing expression of MMPs (36), and tumor invasion and metastasis are often associated with upregulation of MMP-2 and MMP-9 and downregulation of E-cadherin (37); the ERK pathway mediates H-Ras-induced MMP expression (38). Thus, upregulated H-Ras gene expression and protein, an activated ERK pathway, increases of Nox-1, ROS, TNF-α, MMP-2 and MMP-9 and reduced E-cadherin may be regarded as constitutive molecular or biochemical targeted endpoints in PhIP-induced carcinogenesis.

Induction of the epithelial mesenchymal transition program is reportedly involved in cellular acquisition of invasiveness and the plasticity of MCF10A cell transition between epithelial and stem-like cells (39,40). Cancer stem-like cells are postulated to play important roles in generating and maintaining premalignant and malignant lesions (41). Breast cancer stem-like cells express high ALDH activity (26). In addressing whether PhIP-induced carcinogenesis was accompanied by development of cancer stem-like cells, we detected that not only mammospheres, which acquired the ability of serum-independent non-adherent growth but also the ALDH-positive cell population in mammospheres were progressively increased in association with carcinogenesis as detected in MCF10A, P-10, P-20 and MCF10A-Ras cells (Figure 2D). Thus, MCF10A cell carcinogenesis induced by cumulative exposures to PhIP or ectopic expression of oncogenic H-Ras was accompanied by increased stem-like cell populations; the stem-like cell-associated properties of increased ALDH activity and the ability of serum-independent non-adherent growth may be considered as new biochemical and biological targeted endpoints in PhIP-induced carcinogenesis.

These results taken together reveal that cumulative exposures of MCF10A cells to a physiologically achievable dose of PhIP at 10 nmol/l for 20 cycles were sufficient to result in the acquisition of constitutive biological and biochemical targeted endpoints at levels comparable with or modestly lower than their counterparts in tumorigenic MCF10A-Ras cells. However, whether the biochemical changes played roles in maintaining the acquired cancer-associated biological changes for cellular carcinogenesis needs to be clarified.

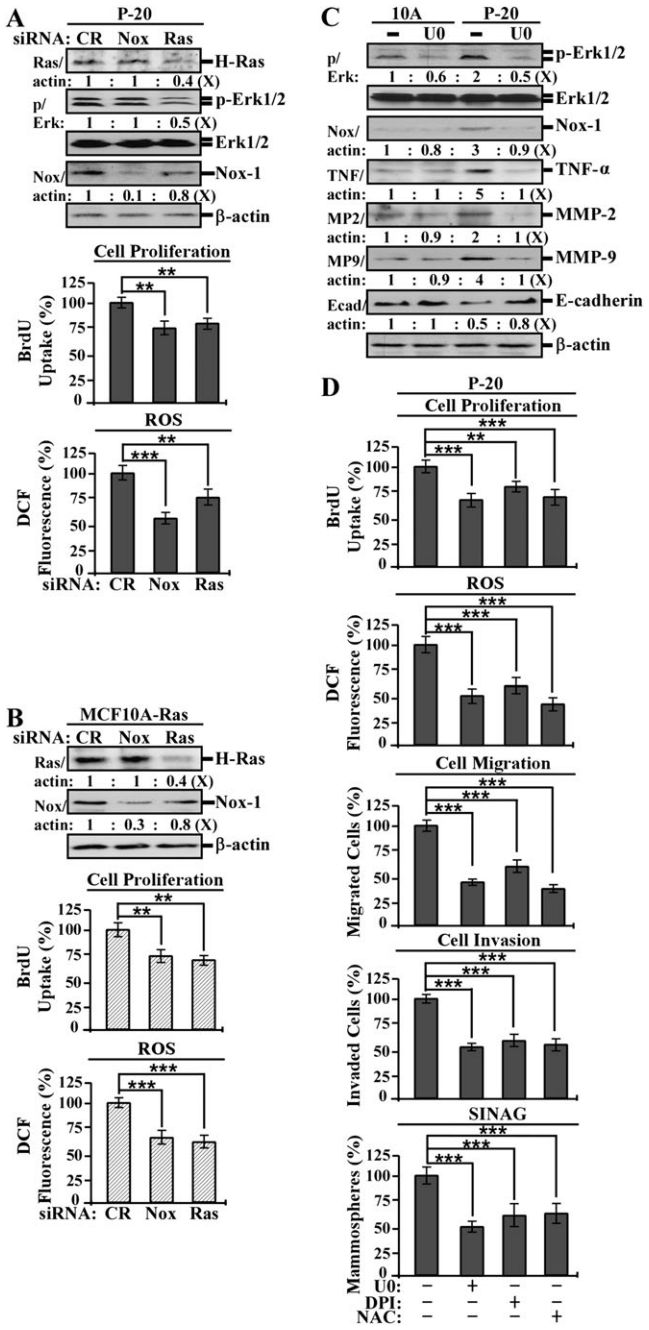

Fig. 3. H-Ras, the ERK pathway, Nox-1 and ROS in modulation of cancer-associated properties. (**A** and **B**) P-20 and MCF10A-Ras cells were transfected with control siRNA (CR) and validated Nox-1- or H-Ras-specific siRNAs for 40 h. (**C**) 10A and P-20 cells were treated with 10 μmol/l U0126 (U0) for 48 h. (**D**) P-20 cells were treated with 10 μmol/l U0, 0.1 μmol/l DPI or 5 mmol/l NAC for 48 h. (A to C) Cell lysates were prepared and analyzed by western immunoblotting to detect levels of H-Ras, p-Erk1/2, Erk1/2, Nox-1, TNF-α, MMP-2, MMP-9 and E-cadherin, with β-actin as a control, and these levels were quantified by densitometry. The levels of H-Ras, Nox-1, TNF-α, MMP-2, MMP-9 and E-cadherin were calculated by normalizing with the level of β-actin, the level set in control cells as 1 (X, arbitrary unit). The level of specific phosphorylation of Erk1/2 (p/Erk) was calculated by normalizing the level of p-Erk1/2 with the level of Erk1/2, then the level set in control cells as 1 (X, arbitrary unit). (A, B and D) Relative proliferation was determined and normalized by the value of 5-bromo-2′-deoxyuridine detected in control siRNA-transfected counterpart cells (A and B) or untreated 10A control cells (D), set as 100%. Relative ROS levels were measured with chloromethyl dichlorodihydrofluorescein diacetate labeling and normalized by fluorescence intensity determined in control cells, set as 100%. (D) Migratory and invasive activities were determined by counting the numbers of cells translocated through a polycarbonate filter without or with coated Matrigel, respectively, in 10 arbitrary visual fields; relative migratory and invasive activities were normalized by the value of migrated or invaded cells detected in untreated cells, respectively, set as 100%. To determine serum-independent non-adherent growth (SINAG), cells were seeded in non-adherent cultures in the absence and presence of 10 μmol/l U0, 0.1 μmol/l DPI or 5 mmol/l NAC for 10 days; then, mammospheres (≥0.1 mm diameter) were counted. Relative mammosphere formations were normalized by the number of mammospheres formed in untreated cells, set as 100%. Columns, mean of triplicates; bars, standard deviation. The Student's *t* test was used to analyze statistical significance, indicated by $^{**}P < 0.01$ and $^{***}P < 0.001$. All results are representative of three independent experiments.

H-Ras, ERK, Nox-1 and ROS in maintenance of cancer-associated properties

Next, we investigated the roles of constitutively upregulated wt H-Ras, a constitutively activated ERK pathway and elevated Nox-1 and ROS in PhIP-transformed cells. We used validated specific siRNAs to knockdown H-Ras and Nox-1, the Mek-specific inhibitor U0126 to block the ERK pathway and the general antioxidant NAC to block ROS production (14). As shown in Figure 3, knockdown of wt H-Ras in P-20 cells (A) or oncogenic H-Ras in MCF10A-Ras cells (B) resulted in reduced levels of phosphorylated Erk1/2 and Nox-1 expression, cell proliferation and ROS, and knockdown of Nox-1 resulted in reduced levels of cell proliferation and ROS. The results indicate that upregulated wt H-Ras played an important role in activation of the ERK pathway and Nox-1 expression, cell proliferation and ROS elevation in PhIP-induced cellular carcinogenesis. In addition, Nox-1 expression was essential for maintaining cell proliferation and ROS elevation.

When blocking the ERK pathway with U0126, the increased Erk1/2 phosphorylation, increased protein levels of Nox-1, TNF-α, MMP-2 and MMP-9 as well as the reduced E-cadherin in P-20 cells (Figure 3C) were reversed. This reversal indicates an essential role of the activated ERK pathway in upregulating Nox-1, TNF-α, MMP-2 and MMP-9 and downregulating E-cadherin.

We also detected that blocking the ERK pathway with U0126, blocking Nox-1 activity with the flavoprotein inhibitor DPI (14) or blocking ROS production with NAC (14) in P-20 cells resulted in significant reductions of cell proliferation, ROS elevation, cell migration, invasion and mammosphere formation (Figure 3D). These results indicate that the ERK pathway, Nox-1 and ROS were essential for maintaining the cancer-associated properties of increased cell proliferation, migration, invasion and serum-independent non-adherent growth acquired by PhIP-transformed cells.

Taken together, these results indicate that constitutive upregulaton of wt H-Ras led to constitutive activation of the ERK pathway to induce downstream Nox-1 and ROS elevation not only leading to induction or downregulation of downstream biochemical events but also contributing to cellular acquisition of cancer-associated properties.

Transient endpoints in PhIP initiation of carcinogenesis

It has been shown that a single exposure of MCF10A cells to PhIP induces transient activation of the ERK pathway, leading to increased cell proliferation and migration and suggesting PhIP as a tumor initiator and promoter in carcinogenesis (16). However, whether this transient activation of the ERK pathway contributed to cellular carcinogenesis induced by long-term exposure needs to be clarified.

Transient increases of H-Ras transcript and protein were induced by PhIP in a single exposure (Figure 4A). Transient activation of the ERK pathway was also induced by PhIP in a single exposure. Blockage of the ERK pathway by U0126 resulted in reducing PhIP-induced Erk1/2 phosphorylation, Nox-1 expression (Figure 4B), cell proliferation and ROS elevation (Figure 4C). Inhibition of Nox-1 and ROS elevation by DPI and NAC, respectively, also resulted in significant reductions of PhIP-induced cell proliferation and ROS elevation (Figure 4C). In addition, we detected that blocking the ERK pathway reduced PhIP-induced H2AX phosphorylation and p53 expression (Figure 4B); increased H2AX phosphorylation and p53 expresson

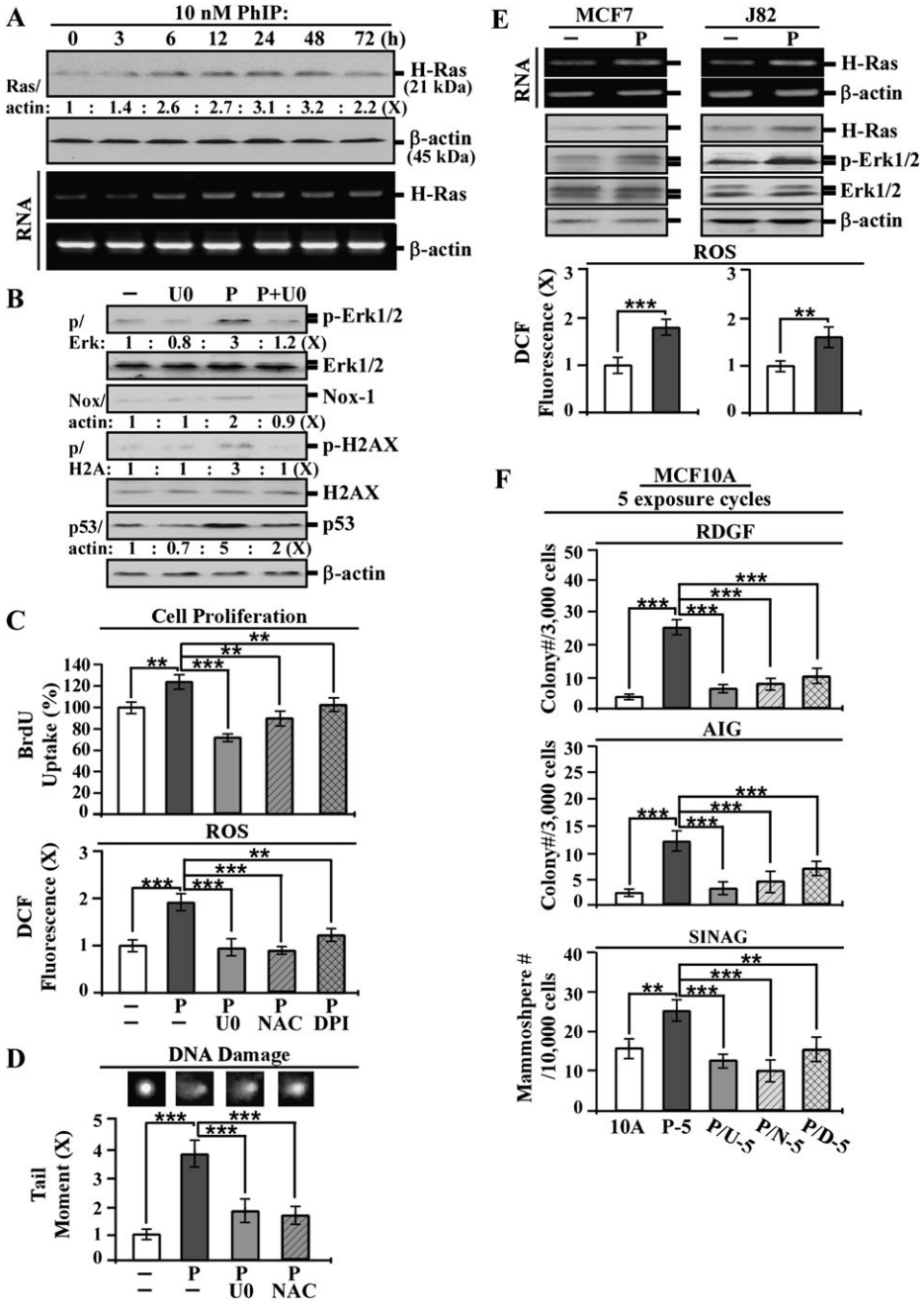

Fig. 4. Role of PhIP-induced transient targeted endpoints of the ERK pathway, cell proliferation, ROS and DNA damage in chronic carcinogenesis. (**A**) MCF10A cells were treated with 10 nmol/l PhIP for the indicated periods. (**B**) MCF10A cells were treated with 10 nmol/l PhIP (P) in the absence or presence of 10 μmol/l U0126 (U0) for 24 h. (**C**) MCF10A cells were treated with 10 nmol/l PhIP in the absence or presence of 10 μmol/l U0, 5 mmol/l NAC or 0.1 μmol/l DPI for 24 h. (**D**) MCF10A cells were treated with 10 nmol/l PhIP in the absence or presence of 10 μmol/l U0 or 5 mmol/l NAC for 24 h. (**E**) MCF7 and J82 cells were treated with 10 nmol/l PhIP for 24 h. (**F**) MCF10A cells were repeatedly exposed to 10 nmol/l PhIP in the absence and presence of 2 μmol/l U0, 5 mmol/l NAC or 0.1 μmol/l DPI for 5 cycles, resulting in P-5, P/U-5, P/N-5 and P/D-5 cell lines, respectively. (A, B and E) Cell lysates were then prepared and analyzed by western immunoblotting to detect levels of H-Ras, p-Erk1/2, Erk1/2, Nox-1, p-H2AX, H2AX and p53, with β-actin as a control, and these levels were quantified by densitometry. The levels of H-Ras, Nox-1 and p53 were calculated by normalizing with the level of β-actin and the level set in untreated control cells as 1 (X, arbitrary unit). The levels of specific phosphorylation of Erk1/2 (p/Erk) and H2AX (p/H2AX) were calculated by normalizing the levels of p-Erk1/2 and p-H2AX with the levels of Erk1/2 and H2AX, respectively, then the level set in control cells as 1 (X, arbitrary unit). (A and E) Total RNAs (RNA) were isolated and analyzed by PCR with specific primers to determine relative gene expression levels of H-Ras, with β-actin as a control. (C) Relative cell proliferation was determined and normalized by the value of 5-bromo-2′-deoxyuridine detected in untreated cells, set as 100%. (C and E) Relative ROS levels were measured with chloromethyl dichlorodihydrofluorescein diacetate labeling and normalized by the fluorescence intensity determined in untreated cells, set as 1 (X, arbitrary unit). (D) Relative DNA damage was measured by a comet assay and normalized by the value of average tail moment determined in untreated counterpart cells, set as 1 (X, arbitrary unit). Representative images of DNA damage in the comet assay are shown. (F) To determine reduced dependence on growth factors (RDGF) and anchorage-independent growth (AIG), cells were maintained in low-mitogen medium for 10 days and seeded in soft agar for 14 days, respectively. Cell colonies (≥0.5 mm diameter) grown in low-mitogen medium and soft agar were counted. To determine serum-independent non-adherent growth (SINAG), cells were seeded in non-adherent cultures for 10 days and mammospheres (≥0.1 mm diameter) were counted. Columns, mean of triplicates; bars, standard deviation. The Student's *t* test was used to analyze statistical significance, indicated by $^{**}P < 0.01$ and $^{***}P < 0.001$. All results are representative of three independent experiments.

are indices of chromosomal DNA damage (42,43). Using a comet assay, we verified that blockage of the ERK pathway or ROS elevation by U0126 and NAC, respectively, reduced PhIP-induced DNA damage (Figure 4D). These results indicate that a single exposure of non-cancerous MCF10A cells to PhIP was able to induce transient activation of the Ras-ERK pathway, leading to Nox-1 expression and ROS elevation and resulting in increased cell proliferation and DNA damage. We detected similar results in breast cancer MCF7 and urinary bladder cancer J82 cells, where PhIP was able to induce the Ras-ERK pathway leading to ROS elevation, indicating that its effects were applicable to other cells (Figure 4E). It has been postulated that activation of the ERK pathway leads to ROS elevation resulting in oxidative DNA damage, contributing to genomic mutations in cellular carcinogenesis (44). However, whether blockage of the PhIP-induced ERK pathway or ROS elevation may suppress cellular carcinogenesis needs to be determined.

Using U0126 to block the ERK pathway, DPI to block Nox-1 activity and NAC to block ROS elevation in each exposure cycle to PhIP, we detected that these blockages resulted in significant inhibition of cellular acquisition of the cancer-associated properties of reduced dependence on growth factors, anchorage-independent growth and mammosphere formation after five exposure cycles (Figure 4F). In contrast, blockage of other pathways, such as phosphoinositide-3-kinase, p38/stress-activated protein kinase or c-jun N-terminal kinase/stress-activated protein kinase, did not result in any reduction of PhIP-induced carcinogenesis (data not shown). Thus, transient induction of the Ras-ERK pathway to ROS elevation was essential for PhIP-induced initiation of cellular carcinogenesis in each single exposure; conceivably, accumulation of PhIP-induced cellular damage contributed to cellular carcinogenesis after cumulative exposures. The Ras-ERK-Nox-ROS pathway, cell proliferation, DNA damage and DNA damage-associated phosphorylation of H2AX may be regarded as transient targeted endpoints for measuring PhIP activity in initiation of cellular carcinogenesis.

Suppression of PhIP-induced carcinogenesis by ECG and EGCG

We detected that ECG and EGCG, at non-cytotoxic concentrations of 10 μg/ml and 5 μg/ml, respectively, reduced PhIP-induced transient induction of the Ras-ERK-Nox-ROS pathway, cell proliferation, H2AX phosphorylation and DNA damage in a single exposure (Figure 5A); however, co-exposure to epicatechin and epigallocatechin at 10 μg/ml failed to reduce these PhIP-induced events (data not

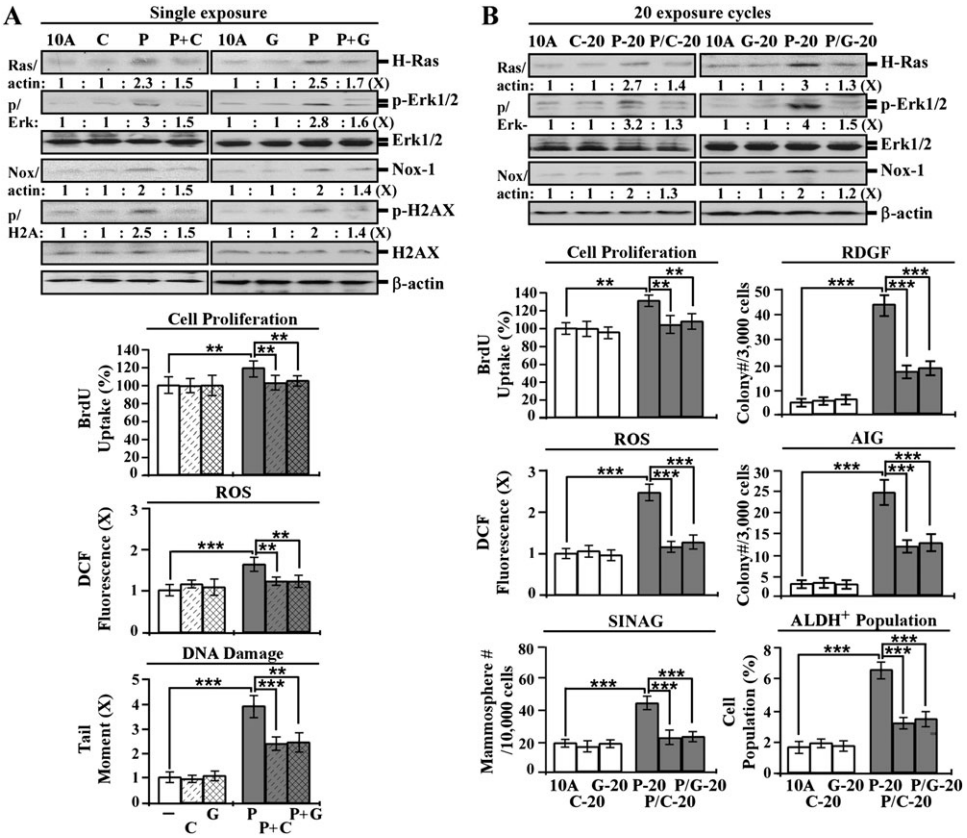

Fig. 5. Intervention of PhIP-induced carcinogenesis by ECG and EGCG. (**A**) MCF10A (10A) cells were treated with 10 nmol/l PhIP (P) in the absence or presence of 10 μg/ml of ECG (C) and 5 μg/ml of EGCG (G) for 24 h. (**B**) 10A cultures were repeatedly exposed to 10 nmol/l PhIP in the absence and presence of 10 μg/ml of ECG and 5 μg/ml of EGCG for 20 cycles, resulting in P-20, C-20, G-20, P/C-20 and P/G-20 cell lines, respectively. Cell lysates were prepared and analyzed by western immunoblotting to detect levels of H-Ras, p-Erk1/2, Erk1/2, Nox-1, with β-actin as a control, and levels were quantified by densitometry. The levels of H-Ras and Nox-1 were calculated by normalizing with the level of β-actin, the level set in control 10A cells as 1 (X, arbitrary unit). The level of specific phosphorylation of Erk1/2 (p/Erk) was calculated by normalizing the level of p-Erk1/2 with the level of Erk1/2, the level set in 10A cells as 1 (X, arbitrary unit). Relative cell proliferation was determined and normalized by the value of 5-bromo-2′-deoxyuridine detected in 10A cells, set as 100%. Relative ROS levels were measured with chloromethyl dichlorodihydrofluorescein diacetate labeling and normalized by the fluorescence intensity determined in 10A cells, set as 1 (X, arbitrary unit). Relative DNA damage was measured by a comet assay and normalized by the value of average tail moment determined in 10A cells, set as 1 (X, arbitrary unit). To determine reduced dependence on growth factors (RDGF) and anchorage-independent growth (AIG), cells were maintained in low-mitogen medium for 10 days and seeded in soft agar for 14 days, respectively. Cell colonies ($\geq$0.5 mm diameter) grown in low-mitogen medium and soft agar were counted. To determine serum-independent non-adherent growth (SINAG), cells were seeded in non-adherent cultures for 10 days, and mammospheres ($\geq$0.1 mm diameter) were counted. Mammospheres were then collected and trypsinized, and ALDH-expressing (ALDH+) cell population (%) was measured by flow cytometry. Columns, mean of triplicates; bars, standard deviation. The Student's *t* test was used to analyze statistical significance, indicated by $^{**}P < 0.01$ and $^{***}P < 0.001$. All results are representative of three independent experiments.

shown), indicating ECG and EGCG were able to block PhIP-induced transient events in a single exposure.

Addressing the activity of ECG and EGCG in blocking chronically induced cellular carcinogenesis, MCF10A cells were exposed to PhIP in the presence of ECG and EGCG for 20 cycles, resulting in P/C-20 and P/G-20 cell lines, respectively, in addition to PhIP-exposed P20, ECG-exposed C-20 and EGCG-exposed G-20 cell lines. We detected that the constantly induced Ras-ERK-Nox-ROS pathway in P-20 cells was suppressed in P/C-20 and P/G-20 cells (Figure 5B). PhIP-induced cellular acquisition of the cancer-associated properties of increased cell proliferation, reduced dependence on growth factors, anchorage-independent growth, mammosphere formation and ALDH activity, as detected in P-20 cells, was significantly reduced by co-exposure to ECG (P/C-20 cells) or EGCG (P/G-20 cells) (Figure 5B). Clearly, non-cytotoxic ECG and EGCG were effective in suppressing PhIP-induced cellular carcinogenesis.

ECG and EGCG suppression of PhIP-induced cellular tumorigenicity

To determine whether cumulative exposures to PhIP were sufficient to induce tumorigenic potency and whether ECG and EGCG were able to suppress this tumorigenicity, MCF10A, PhIP-exposed P-10 and P-20, ECG-protected P/C-20, EGCG-protected P/G-20 and tumorigenic MCF10A-Ras cells were implanted into mammary fat pads of groups of four immune-deficient nude mice. All four mice inoculated with MCF10A-Ras cells developed xenograft tumors by 30 days after inoculation. Two of the four mice inoculated with P-20 cells developed xenograft tumors 60 days after inoculation (Figure 6A, a and b); the 50% incidence of xenograft tumor development indicated a biologically significant increase in tumorigenicity acquisition (45,46). Mice inoculated with MCF10A, P-10 cells, P/C-20 or P/G-20 did not develop any xenograft tumors by 180 days after inoculation. These results indicate that cumulative exposures to PhIP at a physiologically achievable concentration of 10 nmol/l for 10 cycles were insufficient, but exposures for 20 cycles were sufficient to induce biologically significant acquisition of tumorigenicity. However, P-20 cells were less tumorigenic than MCF10A-Ras cells. Also, co-exposure to non-cytotoxic ECG or EGCG was effective in blocking PhIP-induced cellular tumorigenicity.

Histopathologic evaluation of P-20-derived xenograft tumor tissues from mammary sites revealed a well-demarcated expansile population of markedly pleomorphic polygonal cells arranged in lobules of tubulo-acinar structures supported by a fine fibrovascular stroma (Figure 6B, a). The anisocytotic cells had scanted to abundant finely stippled, pale, eosinophilic to vacuolated cytoplasm with euchromatic nuclei and occasional multinucleation. Mitotic figures were frequent (0–10 per ×40 objective field) and occasionally bizarre. There were scattered apoptotic cells and multiple foci of necrosis. These histopathologic features are consistent with mammary adenocarcinoma.

The lymph nodes and lung are the most frequent sites of metastatic mammary adenocarcinoma (47). Although we did not detect any evidence of metastatic cells in the regional lymph nodes, we detected two foci of moderately to markedly pleomorphic polygonal cells arranged in a tubulo-acinar to sheet pattern in the lung from one of the two mice with the mammary xenograft tumor tissue. One focus had a cross sectional diameter of roughly 100 cells (Figure 6B, b), and the second focus was ∼10 cells in diameter. Both foci expanded the interstitium, and the larger focus invested a small vessel. To rule out *de novo* pulmonary tumors in this animal (48), we performed immunohistochemistry to confirm the human origin of these pulmonary masses by their expression of human TNF-α in the P-20 cells. As shown in Figure 6C, cytoplasmic granular brown staining for human TNF-α was appreciably more intense in the epithelial cells of both the primary and pulmonary masses compared with the epithelial cells of adjacent normal mouse mammary glands (Figure 6C, a) and epithelial cells of the alveolar and bronchiolar components of the lung (Figure 6C, b). These results indicated human origin of pulmonary masses and verified the *in vivo* invasive and metastatic potential of P-20 cells in this model.

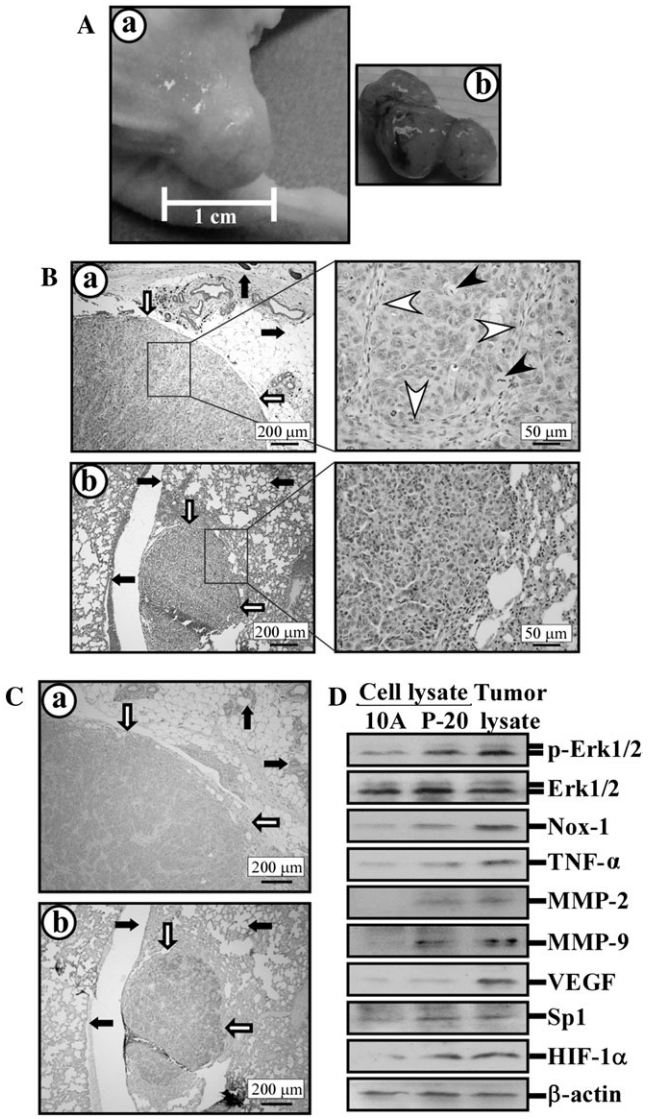

Fig. 6. Cellular tumorigenicity. The P-20 cells were inoculated into the mammary fat pad of nude mice. (**A**) Xenograft tumors developed in the inoculation sites (a); xenograft tumor removed from mouse (b). (**B**) Hematoxylin and eosin-stained histological sections revealed cohesive sheets of neoplastic cells with anaplastic features of primary and metastatic xenograft tumor tissues, as indicated by white arrows, in mammary fat pad (a) and lung (b), respectively. Black arrows indicate mouse tissue. White arrowheads indicate fibrovascular stroma supporting a lobule of tubulo-acinar structure, and black arrowheads indicate mitotic figures. (**C**) Immunohistochemical staining detected human TNF-α in tumor tissues shown in B-a and B-b. White arrows indicate human TNF-α-positive xenograft tumor tissues (brown staining); black arrows indicate mouse tissue. (**D**) Lysates of MCF10A (10A) and P-20 cells and P-20-derived xenograft tumor tissues isolated from mammary fat pads were analyzed by western immunoblotting using specific antibodies to detect levels of p-Erk1/2, Erk1/2, Nox-1, TNF-α, MMP-2, MMP-9, vascular endothelial growth factor (VEGF), Sp1 and HIF-1α, with β-actin as a control. See online Supplementary material for a colour version of this figure.

Analyzing signaling modulators in xenografts, we detected higher levels of phosphorylated Erk1/2, Nox-1, TNF-α, MMP-2, MMP-9, vascular endothelial growth factor, Sp1 and HIF-1α in tumor tissues and P-20 cells versus parental MCF10A cells (Figure 6D), indicating that the ERK pathway and downstream modulators were constantly induced in P-20-derived tumors. Conceivably, metastatic potential was associated with increased MMP-2 and MMP-9 via TNF-α expression, and the potential for angiogenesis was mediated by

vascular endothelial growth factor expression possibly via induction of transcription factors HIF-1α and Sp1.

Discussion

Our model system revealed, for the first time, that cumulative exposures of human breast cells to PhIP at physiologically achievable pico to low nanomolar concentrations induced progressive carcinogenesis from a non-cancerous stage to premalignant and malignant stages in a dose- and exposure-dependent manner. Long-term exposure to low doses of the dietary carcinogen PhIP, through the consumption of well-done meats, may contribute to sporadic breast cancer development. Using various transient and constitutive endpoints as targets, we identified ECG and EGCG, at non-cytotoxic concentrations, effective in suppressing PhIP-induced cellular carcinogenesis and tumorigenicity. Our model system provides a new platform to address targeted intervention of chronically induced breast cell carcinogenesis and suppression by co-exposure to non-cytotoxic preventive agents.

Our model system determines the initiation and progress of cellular carcinogenesis using measurable, transient and constitutive biological, biochemical and molecular changes as targeted endpoints. Transient targeted endpoints are used for measuring the activity of PhIP in initiation of cellular carcinogenesis. Constitutive targeted endpoints are used for measuring the progress of cellular carcinogenesis chronically induced by long-term exposure to PhIP. Using constitutive targeted endpoints, our model revealed that the malignant MCF10A-10nM-P20 cells acquired similar or modestly lower degrees of these endpoints compared with the tumorigenic MCF10A-Ras cells; and the premalignant MCF10A-10nM-P10 cells acquired significantly lower degrees of these endpoints than MCF10A-Ras cells. Hence, our model system, using *in vitro* constitutive biological, biochemical and molecular targeted endpoints, may serve as a platform to predict the *in vivo* tumorigenic potential of carcinogen-exposed cells. For example, PhIP-exposed P-20 cells acquired the targeted endpoints of reduced dependence on growth factors and anchorage-independent growth to degrees comparable with those acquired by MCF10A-Ras cells, indicating that these targeted endpoints may be used to predict cellular acquisition of tumorigenicity. In addition, P-20 cells acquired lower degrees of the targeted endpoints of acinar-conformational disruption, increased cell migration and invasion and increased ability of serum-independent and non-adherent growth than MCF10A-Ras cells, indicating that these targeted endpoints may be used to predict distinguishable degrees of tumorigenic and metastatic potential acquired by carcinogen-exposed cells compared with MCF10A-Ras cells. Thus, by further determining the value of individual and grouped, *in vitro* targeted endpoints, our model will provide an accurate cost-efficient platform to initially predict the tumorigenic and metastatic potential of carcinogen-exposed cells and to subsequently verify this potential in *in vivo* animal studies.

PhIP is able to induce a high frequency of activation–mutation in the H-*ras* gene in animal mammary tumors (12). The contributing role of mutationally activated Ras has been widely recognized in human cancers (17). However, although aberrant upregulation of wt H-*ras* gene expression has been detected in >50% of premalignant and malignant breast lesions isolated from human patients (49,50), the role of upregulated wt H-Ras in the development of premalignant and malignant breast lesions was unclear. Apparently, upregulation of the wt H-*ras* gene was overlooked in past studies of carcinogenesis. Our model revealed, for the first time, an important role of transiently and constitutively upregulated wt H-Ras in regulating downstream signaling modulators for PhIP-induced initiation and maintenance of breast cell carcinogenesis. However, the mechanisms for PhIP-induced transient and constant wt H-Ras upregulation in breast cells remain to be studied.

Using transient targeted endpoints in initial screening of preventive agents and constitutive targeted endpoints in subsequent validation of effective preventive agents, our model system may provide a sensitive platform to help accelerate the identification of non-cytotoxic preventive agents effective in targeted intervention of carcinogenesis as well as tumorigenesis associated with chronic exposure to environmental carcinogens. Thereby, our model system may be a tool that will contribute to future studies for reducing the health risk of sporadic breast cancer.

Funding

This work was supported by the University of Tennessee, College of Veterinary Medicine, Center of Excellence in Livestock Diseases and Human Health (to H.-C.R.W.) and the National Institutes of Health (CA129772 to H.-C.R.W.).

Acknowledgements

We are grateful to Ms. D.J. Trent for technique support in flow cytometric analysis and Ms. M. Bailey for textual editing of the manuscript.

Conflict of Interest Statement: None declared.

References

1. Gray,J. *et al*. (2009) State of the evidence: the connection between breast cancer and the environment. *Int. J. Occup. Environ. Health*, **15**, 43–78.
2. DeBruin,L.S. *et al*. (2002) Perspectives on the chemical etiology of breast cancer. *Environ. Health Perspect.*, **110**, 119–128.
3. Kelloff,G.J. *et al*. (eds.) (2005) *Cancer Chemoprevention: Strategies for Cancer Chemoprevention*. **Vol. 2**. Human Press, Totowa, NJ.
4. Mehta,R.G. (2000) Experimental basis for the prevention of breast cancer. *Eur. J. Cancer*, **36**, 1275–1282.
5. Rudel,R.A. *et al*. (2007) Chemicals causing mammary gland tumors in animals signal new directions for epidemiology, chemicals testing, and risk assessment for breast cancer prevention. *Cancer*, **109**, 2635–2666.
6. Pala,V. *et al*. (2009) Meat, eggs, dairy products, and risk of breast cancer in the European Prospective Investigation into Cancer and Nutrition (EPIC) cohort. *Am. J. Clin. Nutr.*, **90**, 602–612.
7. Zheng,W. *et al*. (2009) Well-done meat intake, heterocyclic amine exposure, and cancer risk. *Nutr. Cancer*, **61**, 437–446.
8. Sugimura,T. *et al*. (2004) Heterocyclic amines: mutagens/carcinogens produced during cooking of meat and fish. *Cancer Sci.*, **95**, 290–299.
9. Zheng,W. *et al*. (1998) Well-done meat intake and the risk of breast cancer. *J. Natl Cancer Inst.*, **90**, 1724–1729.
10. Sinha,R. *et al*. (2000) 2-Amino-1-methyl-6-phenylimidazo[4,5-*b*]pyridine, a carcinogen in high-temperature-cooked meat, and breast cancer risk. *J. Natl Cancer Inst.*, **92**, 1352–1354.
11. Zhu,J. *et al*. (2003) Detection of 2-amino-1-methyl-6-phenylimidazo[4,5-*b*]-pyridine-DNA adducts in normal breast tissues and risk of breast cancer. *Cancer Epidemiol. Biomarkers Prev.*, **12**, 830–837.
12. Yu,M. *et al*. (2002) H-ras oncogene mutations during development of 2-amino-1-methyl-6-phenylimidazo[4,5-b]pyridine (PhIP)-induced rat mammary gland cancer. *Carcinogenesis*, **23**, 2123–2128.
13. Moon,A. *et al*. (2000) H-ras, but not N-ras, induces an invasive phenotype in human breast epithelial cells: a role for MMP-2 in the H-ras-induced invasive phenotype. *Int. J. Cancer*, **85**, 176–181.
14. Choudhary,S. *et al*. (2010) FK228 and oncogenic H-Ras synergistically induce Mek1/2 and Nox-1 to generate reactive oxygen species for differential cell death. *Anticancer Drugs*, **21**, 831–840.
15. Bedard,K. *et al*. (2007) The NOX family of ROS-generating NADPH oxidases: physiology and pathophysiology. *Physiol. Rev.*, **87**, 245–313.
16. Creton,S.K. *et al*. (2007) The cooked meat carcinogen 2-amino-1-methyl-6-phenylimidazo[4,5-b]pyridine activates the extracellular signal regulated kinase mitogen-activated protein kinase pathway. *Cancer Res.*, **67**, 11455–11462.
17. Campbell,S.L. *et al*. (1998) Increasing complexity of Ras signaling. *Oncogene*, **17**, 1395–1413.
18. Mei,J. *et al*. (2003) Transformation of noncancerous human breast epithelial cell MCF10A induced by the tobacco-specific carcinogen NNK. *Breast Cancer Res. Treat*, **79**, 95–105.
19. Siriwardhana,N. *et al*. (2008) Precancerous carcinogenesis of human breast epithelial cells by chronic exposure to benzo[a]pyrene. *Mol. Carcinog.*, **47**, 338–348.
20. Siriwardhana,N. *et al*. (2008) Precancerous model of human breast epithelial cells induced by the tobacco-specific carcinogen NNK for prevention. *Breast Cancer Res. Treat.*, **109**, 427–441.
21. Song,X. *et al*. (2010) Grape seed proanthocyanidin suppression of breast cell carcinogenesis induced by chronic exposure to combined

4-(methylnitrosamino)-1-(3-pyridyl)-1-butanone and benzo[a]pyrene. *Mol. Carcinog.*, **49**, 450–463.
22. Rathore,K. *et al*. (2011) Green tea catechin intervention of reactive oxygen species-mediated ERK pathway activation and chronically-induced breast cell carcinogenesis. *Carcinogenesis,*, **33**, 174–183.
23. Yang,C.S. *et al*. (2009) Cancer prevention by tea: animal studies, molecular mechanisms and human relevance. *Nat. Rev. Cancer*, **9**, 429–439.
24. Choudhary,S. *et al*. (2007) Proapoptotic ability of oncogenic H-Ras to facilitate apoptosis induced by histone deacetylase inhibitors in human cancer cells. *Mol. Cancer Ther.*, **6**, 1099–1111.
25. Albini,A. *et al*. (1987) A rapid *in vitro* assay for quantitating the invasive potential of tumor cells. *Cancer Res.*, **47**, 3239–3245.
26. Ginestier,C. *et al*. (2007) ALDH1 is a marker of normal and malignant human mammary stem cells and a predictor of poor clinical outcome. *Cell Stem Cell*, **1**, 555–567.
27. Olive,P.L. *et al*. (2006) The comet assay: a method to measure DNA damage in individual cells. *Nat. Protoc.*, **1**, 23–29.
28. Hanahan,D. *et al*. (2000) The hallmarks of cancer. *Cell*, **100**, 57–70.
29. Larsson,O. *et al*. (1985) Consequences of parental exposure to serum-free medium for progeny cell division. *J. Cell Sci.*, **75**, 259–268.
30. Reddig,P.J. *et al*. (2005) Clinging to life: cell to matrix adhesion and cell survival. *Cancer Metastasis Rev.*, **24**, 425–439.
31. Datta,S. *et al*. (2007) Bmi-1 cooperates with H-Ras to transform human mammary epithelial cells via dysregulation of multiple growth-regulatory pathways. *Cancer Res.*, **67**, 10286–10295.
32. Debnath,J. *et al*. (2005) Modelling glandular epithelial cancers in three-dimensional cultures. *Nat. Rev. Cancer*, **5**, 675–688.
33. Preston-Martin,S. *et al*. (1993) Epidemiologic evidence for the increased cell proliferation model of carcinogenesis. *Prog. Clin. Biol. Res.*, **369**, 21–34.
34. Adachi,Y. *et al*. (2008) Oncogenic Ras upregulates NADPH oxidase 1 gene expression through MEK–ERK-dependent phosphorylation of GATA-6. *Oncogene*, **27**, 4921–4932.
35. Suh,Y.A. *et al*. (1999) Cell transformation by the superoxide-generating oxidase Mox1. *Nature*, **401**, 79–82.
36. Montesano,R. *et al*. (2005) Tumour necrosis factor alpha confers an invasive, transformed phenotype on mammary epithelial cells. *J. Cell Sci.*, **118**, 3487–3500.
37. Herbst,R.S. *et al*. (2000) Differential expression of E-Cadherin and type IV collagenase genes predicts outcome in patients with stage I non-small cell lung carcinoma. *Clin. Cancer Res.*, **6**, 790–797.
38. Lecureur,V. *et al*. (2005) ERK-dependent induction of TNFalpha expression by the environmental contaminant benzo(a)pyrene in primary human macrophages. *FEBS Lett.*, **579**, 1904–1910.
39. Sarrió,D. *et al*. (2008) Epithelial-mesenchymal transition in breast cancer relates to the basal-like phenotype. *Cancer Res.*, **68**, 989–997.
40. Gupta,P.B. *et al*. (2009) Cancer stem cells: mirage or reality? *Nat. Med.*, **15**, 1010–1012.
41. Charafe-Jauffret,E. *et al*. (2008) Cancer stem cells in breast: current opinion and future challenges. *Pathobiology*, **75**, 75–84.
42. Liu,Y. *et al*. (2001) p53 protein at the hub of cellular DNA damage response pathways through sequence-specific and non-sequence-specific DNA binding. *Carcinogenesis*, **22**, 851–860.
43. Rogakou,E.P. *et al*. (1998) DNA double-stranded breaks induce histone H2AX phosphorylation on serine. *J. Biol. Chem.*, **139**, 5858–5868.
44. Cooke,M.S. *et al*. (2003) Oxidative DNA damage: mechanisms, mutation, and disease. *FASEB J.*, **17**, 1195–1214.
45. Gart,J.J. *et al*. (1979) Statistical issues in interpretation of chronic bioassay tests for carcinogenicity. *J. Natl Cancer Inst.*, **62**, 957–974.
46. Cohrssen,J.J. *et al*. (1989) *Risk Analysis: A Guide to Principles and Methods for Analyzing Health and Environmental Risks*. Diane Publishing Co, Darby, PA.
47. Price,J.E. *et al*. (1990) Tumorigenicity and metastasis of human breast carcinoma cell lines in nude mice. *Cancer Res.*, **50**, 717–721.
48. Sharkey,F.E. *et al*. (1979) Incidence and pathological features of spontaneous tumors in athymic nude mice. *Cancer Res.*, **39**, 833–839.
49. Hand,P.H. *et al*. (1987) Quantitation of Harvey ras p21 enhanced expression in human breast and colon carcinomas. *J. Natl Cancer Inst.*, **79**, 59–65.
50. Pethe,V. *et al*. (1999) Estrogen inducibility of c-Ha-ras transcription in breast cancer cells. Identification of functional estrogen-responsive transcriptional regulatory elements in exon 1/intron 1 of the c-Ha-ras gene. *J. Biol. Chem.*, **274**, 30969–30978.

Received November 2, 2011; revised January 27, 2012;
accepted February 1, 2012